

Outer gap accelerator closed by magnetic pair-creation process

J. Takata¹, Y.Wang² and K.S. Cheng³

Department of Physics, University of Hong Kong, Pokfulam Road, Hong Kong

Received _____; accepted _____

¹takata@hku.hk

²yuwang@hku.hk

³hrspksc@hkucc.hku.hk

ABSTRACT

We discuss outer gap closure mechanism in the trans-field direction with the magnetic pair-creation process near the stellar surface. The gap closure by the magnetic pair-creation is possible if some fraction of the pairs are produced with an outgoing momentum. By assuming that multiple magnetic field will affect the local field near the stellar surface, we show a specific magnetic field geometry near the stellar surface resulting in the outflow of the pairs. Together with the fact that the electric field is weak below null charge surface, the characteristic curvature photon energy emitted by incoming particles, which were accelerated in the outer gap, decreases drastically to $\sim 100\text{MeV}$ near the stellar surface. We estimate the height measured from the last-open field line, above which 100 MeV photons is converted into pairs by the magnetic pair-creation. We also show the resultant multiplicity due to the magnetic pair-creation process could acquire $M_{e\pm} \sim 10^4 - 10^5$. In this model the fractional outer gap size is proportional to $P^{-1/2}$. The predicted gamma-ray luminosity (L_γ) and the characteristic curvature photon energy (E_c) emitted from the outer gap are proportional to $B^2P^{-5/2}$ and $B^{3/4}P^{-1}$ respectively. This model also predicts that L_γ and E_c are related to the spin down power (L_{sd}) or the spin down age of pulsars (τ) as $L_\gamma \propto L_{sd}^{5/8}$ or $L_\gamma \propto \tau^{-5/4}$, and $E_c \propto L_{sd}^{1/4}$ or $E_c \propto \tau^{-1/2}$ respectively.

Subject headings: pulsars: general– radiation mechanisms:non-thermal– -gamma rays:theory–magnetic field

1. Introduction

The mechanism of particle acceleration and high-energy emission processes in the pulsar magnetospheres are one of the unresolved physics of the pulsar activities. The particle acceleration process and resultant high-energy γ -ray emission process have been discussed with the polar cap model (Ruderman & Sutherland 1975; Daugherty & Harding 1982), the slot gap model (Arons 1981; Harding, Usov & Muslimov 2005; Harding et al. 2008) and the outer gap model (Cheng, Ho & Ruderman 1986a,b; Hirovani 2008; Takata & Chang 2009). The polar cap model assumes the emission site close to the stellar surface above the polar cap, and the slot gap and the outer gap models assume the emission site in the outer magnetosphere. The different acceleration models have predicted the different properties of the γ -ray emissions from the pulsar magnetospheres.

The observations of the pulsar emitting electromagnetic radiation in the high-energy γ -ray bands have been facilitated by recent space and ground based telescopes. In particular, the *Fermi* γ -ray telescope has measured the γ -ray emissions from ~ 46 pulsars (Abdo et al. 2010, 2009a,b), including 21 radio-loud, 17 radio-quiet and 8 millisecond pulsars. In addition, *AGILE* (Astro-rivelatore Gamma a Immagini LEggero) has also reported the detection of γ -ray emissions from 4 new pulsars with 4 candidates (Pellizzoni et al. 2009). In more higher energy regime, *MAGIC* (Major Atmospheric Gamma Imaging Cherenkov) telescope has detected for the first time pulsed gamma-ray radiation above 25 GeV from the Crab pulsar (Aliu et al. 2008). These observations will be useful to discriminate between the emission models. For example, the *Fermi* telescope has measured the spectral properties above 10 GeV with a better sensitivity than *EGRET*. It was found that the spectral shape of γ -ray emissions from the Vela pulsar is well fitted with a power law (photon index $\Gamma \sim 1.5$) plus exponential cut-off ($E_{cut} \sim 3$ GeV) model. The discovered exponential cut-off feature predicts that the emissions from the outer magnetosphere (Abdo

et al. 2009c) is more favored than the polar cap region (Daugherty & Harding 1996), which predicts a super exponential cut-off with the magnetic pair-creation. Furthermore, the detection of the radiation above 25 GeV bands associated with the Crab pulsar has also predicted the high-energy emission in the outer magnetosphere (Aliu et al. 2008).

The pulse profiles observed by the *Fermi* telescope allow us to study the site of the γ -ray emissions in the pulsar magnetosphere. Venter et al. (2009) fitted the pulse profiles of the 8 millisecond pulsars with the geometries predicted by the different emission models. They showed that most of the pulse profiles can be best fit with the outer gap (Takata et al. 2007; Takata & Chang 2007; Tang et al. 2008) or the two pole caustic (Dyks & Rudak 2003; Dyks et al. 2004) geometries, which have a slab like geometry along the last-open field lines. However, they also found that the pulse profiles of two out of eight millisecond pulsars cannot be fitted by either the geometries with the outer gap or the caustic models. They proposed a pair-starved polar cap model, in which the multiplicity of the pairs is not high enough to completely screen the electric field above the polar cap, and the particles are continuously accelerated up to high altitude over full open field line region.

The increase of the γ -ray pulsars allows us to perform a detail statistical study of the γ -ray pulsars. In particular, the *Fermi* γ -ray pulsars including millisecond pulsars will reveal the relation between the γ -ray luminosity (L_γ) and the spin down power (L_{sd}), for which $L_\gamma \propto L_{sd}^\beta$ with $\beta \sim 0.5 - 0.6$ was predicted by *EGRET* measurements (Thompson 2004). Also, the *Fermi* γ -ray pulsars will enable us to discuss the general trend of the relation among the spectral properties of the γ -ray emissions (e.g. the cut-off energy and photon index) and the pulsar parameters (e.g. rotation period and surface magnetic field). Together with the observed pulse profiles and the spectra, these general properties of the γ -ray emissions will discriminate between the γ -ray emission models in the pulsar magnetospheres.

In this paper, we discuss the γ -ray emissions from the outer gap accelerator. We propose a new outer gap closure mechanism by the magnetic pair-creation process near the stellar surface. The pairs produced by the magnetic pair creation will be able to close the gap if the sufficiently strong surface multiple field exists and affects the dipole field near the surface. In section 2, we first summarize results of gap closure process by photon-photon pair-creation process, and then we discuss our new gap closure mechanism by the magnetic pair-creation process. In section 3, we describe the model predictions of the properties of the γ -ray emissions. In section 4, we will compare the model predictions with the results of the *Fermi* observations. We also discuss applicability of our model. In section 5, we will summarize our gap closure model and predictions for the outer gap accelerator.

2. Gap closure mechanism

2.1. Photon-photon pair-creation process

The outer gap accelerator model was proposed by Cheng, Ho and Ruderman (1986a,b), who argued that a large global current flow through the outer magnetosphere causes a charge depletion from the Goldreich-Julian charge density, which is defined by $\rho_{GJ} = -\vec{\Omega} \cdot \vec{B}/2\pi c$ (Goldreich & Julian 1969) with $\vec{\Omega}$ being the vector of the rotation axis and \vec{B} the magnetic field. In the charge depletion region, the non-corotational electric field along the magnetic field accelerates the charged particles, which result in the high energy γ -ray emissions. This non-corotational electric field could be screened out by the discharge of the copious electron and positron pairs produced by the pair-creation process of the γ -ray photons. The outer gap would be completely screened out in the trans-field direction, where the non-corotational electric field perpendicular to the magnetic field in the poloidal plane is equal to zero. This condition implies that the total potential (corotational + non-corotational) field is continuously connected to the corotational field outside the outer gap.

Zhang & Cheng (1997) discussed the gap closure mechanism by the photon-photon pair-creation process between the high-energy γ -rays emitted in the gap and the X-rays coming from the stellar surface. They estimated the typical gap thickness from the pair-creation condition $E_\gamma E_X \sim 2(m_e c^2)^2$, where E_γ is the energy of the emitted γ -ray photons in the outer gap and E_X is the energy of the soft-photons from the stellar surface, and they obtained the fractional gap thickness as $f_p \equiv h_\perp(R_{lc}/2)/R_{lc} \sim 5.5 P^{26/21} B_{d,12}^{-4/7}$, where R_{lc} is the light cylinder radius, $h_\perp(R_{lc}/2)$ is the gap thickness in poloidal plane at $r = R_{lc}/2$ and $B_{d,12}$ is the global stellar magnetic field in units of 10^{12} Gauss.

The outer gap closure mechanism with the photon-photon pair-creation process in the trans-field direction have also been discussed by solving the electrodynamics in the outer gap with 2-dimensional and 3-dimensional geometry (Takata, Shibata and Hirotani 2004; Hirotani 2006a,b; Hirotani 2008). For example, Hirotani (2006a) demonstrated that the outer gap for the young pulsar, the Crab pulsar, is almost screened out in the trans-field direction at the fractional gap thickness of $f \sim 0.2$ (figure 6 in Hirotani 2006a). For mature pulsars such like Geminga, on the other hand, Takata and Chang (2009) argued that the photon-photon pair-creation process will be insufficient in the outer magnetosphere and the outer gap could occupy entire region between the last-open field lines and the critical field lines that have the null charge point at the light cylinder.

2.2. New gap closure mechanism; magnetic pair-creation process near the stellar surface

In this paper, we propose a possible gap closure mechanism, in which the magnetic pair-creation process near the stellar surface supplies the electron and positron pairs to close the outer gap in the trans-field direction. It has been proposed that the magnetic field near the stellar surface is enhanced by the strong multiple magnetic field, although the

global magnetic field is well described by the dipole field (Blandford et al. 1983; Romani 1990; Ruderman 1991). The neutron star magnetic field will be produced by a current flowing the crust, which has a thickness of $\delta r \sim 1 - 3 \times 10^5 \text{ cm} \ll R_s$. It was suggested that the magnetic structure near the stellar surface is super position of clumps resolved into multiples of characteristic of the order of $R_s/\delta r$ (Arons 1993; Zhang & Cheng 2003). If the clumps cover whole stellar surface, the strength of the stellar magnetic field is order of $B_s \sim (R_s/\delta r)^n B_d$, where B_d is the strength of dipole magnetic field determined by the observed rotation period P and the period derivative \dot{P} , and $n = 1$ and 2 represent coherent and incoherent superposition of the magnetic momentum of the clump, respectively. This model indicates the strength of the stellar magnetic field can take easily $B_s \sim 10 - 100 B_d$. Therefore, even in the millisecond pulsar, the magnetic field near the star surface will be close to $B_s \sim 10^{11}$ Gauss, and the magnetic pair-creation process will take place close to the stellar surface.

We will argue that the γ -rays emitted near the stellar surface is converted into the pairs via the magnetic pair-creation process above the height ($h_{\perp,m}$) measured from the last-open field line. In equation (6), we will estimate the height, $h_{\perp,m}$, above which the pair-creation process takes place. The important conditions for closing the outer gap by the pairs produced by the magnetic pair-creation process near the stellar surface are as follows; (1) the gap was not closed by the photon-photon pair-creation process below the height $h_{\perp,m}$ (c.f. section 4.2), (2) the local magnetic field lines near the stellar surface is bending away from the last-open field lines (see below and Figure 2) due to the strong multiple fields, and (3) some of magnetic pairs migrate into outer magnetosphere. The second condition is required to produce outflows of the magnetic pairs.

Figure 1 and 2 represent the schematic view of the outer magnetosphere and of the magnetic structure near the stellar surface, which is favored in this study, respectively. In

the outer magnetosphere, the photon-photon pair-production process create pairs, which are separated by the accelerating electric field. Inward propagating particles will emit the γ -ray photons toward the strong magnetic field region near the stellar surface. As demonstrated by the electrodynamic study (e.g. Hirotani 2006a), the electric field below null charge surface are significantly reduced by the pairs and arises with a very weak field. Below the null charge surface, therefore, the curvature energy loss will not be able to be compensated by the acceleration of the electric field in the gap (c.f. section 4.3), and the incoming particles loose their energy by the curvature radiation. It is interesting to note that there is a minimum energy of the curvature photons, which does not depend on any pulsar parameters and the curvature radius of the local magnetic field. Assuming that the curvature loss dominates the energy gain due to the acceleration by the electric field, the evolution of the Lorentz factor may be described as

$$m_e c^2 \frac{d\gamma}{dt} = -\frac{2}{3} \gamma^4 \frac{e^2 c}{s^2}, \quad (1)$$

where s is the curvature radius. Close to the null charge surface, the incoming particles lose their energy with a time scale smaller than the time scale of travelling to the stellar surface, because the Lorentz factor is high enough. As decreasing the Lorentz factor of the particles, the curvature energy loss time scale becomes comparable to the crossing time scale of $dt \sim s/c$. In such a case, equation of motion (1) implies $1/\gamma^2 - 1/\gamma_0^2 \sim 4e^2/3m_e c^2$ where γ_0 is the initial Lorentz factor. If $\gamma \ll \gamma_0$, the typical Lorentz factor of the particles below the null charge surface becomes

$$\gamma \sim \left(\frac{3m_e c^2 s}{4e^2} \right)^{1/3} \sim 3 \times 10^6 s_7^{1/3}, \quad (2)$$

where s_7 is the curvature radius in units of 10^7 cm.

The Lorentz factor (2) gives the minimum energy of the curvature photons, which does

not depend on any pulsar parameters, that

$$E_{min} \sim \frac{3 \hbar \gamma^3 c}{4 s} \sim \frac{9 m_e c^2}{8 \alpha_f} \sim 77 \text{ MeV}, \quad (3)$$

where α_f is the fine structure constant. We expect that the incoming electrons will mainly emit the curvature photons with an energy $E_{min} \sim 100$ MeV between the stellar surface and the null charge surface. Some of 100 MeV photons emitted below the null charge surface pass through vicinity of the stellar surface. Applying the static dipole field geometry and $P = 0.1$, for example, the trajectory of the 100 MeV photons emitted below $r \sim 10^7$ cm on the last-open field line will cross the magnetic pole below $r \sim 2 \times 10^6$ cm. Therefore, it is expected almost all 100 MeV photons emitted below $r \sim 10^7$ cm will be converted into pairs with a strong magnetic field of $B \sim 10^{11} - 10^{13}$ Gauss. We find that an incoming particle emits about $N \sim 2 \times 10^4 s_7^{-2/3}$ photons before reaching the stellar surface below $r \sim 10^7$ cm .

For the millisecond pulsars, the 100 MeV curvature photons could be converted into the pairs with a strong multiple magnetic field, which could acquire $B_s \sim 10^{11}$ Gauss, at very close to the stellar surface. With the static dipole field geometry, the curvature photons emitted below $r \sim 3 \times 10^6$ cm is propagating toward the magnetic pole for the typical rotation period of $P = 4$ ms. An incoming particle will emit $N \sim 10^4 s_6^{-2/3}$ of ~ 100 MeV photons below $r \sim 3 \times 10^6$ cm

For the canonical pulsar, the pairs created by the magnetic pair-creation process of 100 MeV photons can also emit the soft γ -rays via the synchrotron radiation, which may further generate new pairs. With the typical Lorentz factor of $\Gamma \sim 100$, one pair emits about 1~10 synchrotron photons with a typical energy of $E_{syn} \sim 5(\Gamma/100)^2(\sin \theta_a/0.05)(B/5 \cdot 10^{11} \text{ G}) \text{ MeV}$. This ~ 5 MeV synchrotron photons also could be converted into pairs with a strong local magnetic field $10^{12} \sim 10^{13}$ Gauss near the stellar surface, where the magnetic field will be enhanced by the multiple magnetic field. This implies the resultant multiplicity of an incoming particles, which was accelerated in the

outer gap, could be $M_{e\pm} \sim 10^5 s_7^{-2/3}$ for the canonical pulsars.

The mean free path of the magnetic pair-creation process of the photon with the energy E_γ is described as (Erber 1966; Ruderman & Surtherland 1975)

$$l_m = \frac{4.4}{\alpha_f} \frac{\hbar}{m_e c} \frac{B_q}{B_\perp} \exp\left(\frac{4}{3\chi}\right), \quad (4)$$

where $\chi = E_\gamma B_\perp / 2m_e c^2 B_q$, $B_q = 4.4 \times 10^{13}$ Gauss and $B_\perp = B \sin \theta_a$ with θ_a is the angle between the direction of the propagating for the photon and the magnetic field. The exponential dependency of the mean-free path on the photon energy E_γ and the angle θ_a implies that most of emitted photons will be converted into pairs if the condition that $E_\gamma B_\perp / (2m_e c^2 B_q) \sim \chi$ is satisfied. Using the magnetic pair-creation condition, we can estimate height measured from the last open field line, above which the magnetic pair-creation process of the photons with $E_{min} \sim 100$ MeV becomes important process. The collision angle θ_a is approximately described as

$$\sin \theta_a \sim \frac{\ell}{s} \sim \sqrt{\frac{2h_\perp}{s}}, \quad (5)$$

where $\ell \sim \sqrt{2h_\perp s}$ is the propagating distance of a photon from the emission point, and h_\perp is height measured from the last-open field line. The magnetic pair-creation condition implies that the curvature photons with an energy ~ 100 MeV will be converted into the pairs above the height

$$h_{\perp,m}(R_i) \sim 10^4 \chi_{-1}^2 B_{m,12}^{-2} s_7 \text{ cm}, \quad (6)$$

where R_i expresses the critical radial distance below which the magnetic pair-creation process becomes to be important and it will be $R_i \sim 2 - 3R_s$ for the canonical pulsars and $R_i \sim R_s$ for the millisecond pulsars. In addition, $\chi_{-1} = \chi/0.1$, $B_{m,12}$ is the strength of the magnetic field at the pair-creation position in units of 10^{12} Gauss, and we used $E_{min} = 100$ MeV. Rescaling the thickness at the stellar radius using the magnetic flux conservation, we obtain $h_{\perp,m}(R_s) \sim (R_s/R_i)^{3/2} h_{\perp,m}(R_i)$ with R_s being the stellar radius.

As we have discussed above, the incoming particles will create pairs above the height $h_{\perp,m}$, which is described by equation (6), via the magnetic pair-creation process near the stellar surface, and the multiplicity could acquire $M_{e\pm} \sim 10^4 - 10^5$ for the canonical pulsars and $\sim 10^4$ for the millisecond pulsars. Although it is expected most of the created pairs have inward momentum and migrate toward the star, it may be possible that small fraction of the created pairs are produced with an outgoing momentum and migrate into outer magnetosphere, as discussed below. In fact, about ~ 10 pairs out of $M_{e\pm} \sim 10^4 - 10^5$ will be enough to close the outer gap accelerator in the trans-field direction everywhere in the outer magnetosphere.

The magnetic pairs would be produced with an outgoing momentum if the magnetic structure near the stellar surface is affected by the strong multiple field, as illustrated in Figure 2, which shows how some pairs can acquire the outgoing momentum due to the geometry of the local magnetic field lines. In fact, it is required that the magnetic field (thick dashed-lines) on the pair-creation points are bending away from the last-open field line due to a strong multiple field (solid-dashed line). The solid curved lines represent the global field which are not affected by the local magnetic field, and thin dashed-lines represent the geometry without the multiple field. The 100 MeV curvature photons (solid arrows) emitted by the incoming particles, which were accelerated inside the outer gap, are converted into the pairs via the magnetic pair-creation above height, $h_{\perp,m}$ described by equation (6). For the canonical pulsars, the synchrotron radiation of the created pairs will produces ~ 5 MeV photons (dashed arrows), which could be converted into new pairs by a strong magnetic field near the stellar surface. If the direction of the magnetic field at the pair-creation positions is bending away from the last-open field line, it is possible that the collision angle (denoted as α in the Figure 2) between the photons and the magnetic field line becomes larger than $\alpha \geq 90^\circ$, implying the created pair has the outgoing momentum.

We note that (1) because the position of the pair-creation point is determined by the value $B \sin \alpha$, and (2) because the collision angle changes from a smaller value to a larger value as the photon propagate toward the stellar surface, the position with the collision angle smaller than 90° is preferentially chosen as the pair-creation point, although $\sin \alpha$ gives the same values with, for example, $\alpha = 80^\circ$ and 110° . However, the magnetic field also increases as the photons propagate toward the stellar surface, implying the strength of the magnetic field is bigger for the position with $\alpha = 110^\circ$ than that with $\alpha = 80^\circ$. As a result, it will be possible that some photons do not have enough energy to produce the pairs with the magnetic field at the position with $\alpha = 80^\circ$, but do to produce the pairs at the position with $\alpha = 110^\circ$. On these ground, some created pairs will be able to have the outgoing momentum, if the local magnetic field is bending away from the last-open field line.

With the magnetic field structure bending away from the last-open field line, the incoming particles from the outer gap could emit the 100 MeV curvature photons toward lower altitude, and therefore could make pairs at lower altitude, implying the magnetic pair-creation process could occur inside the gap if the inner boundary is located close to the stellar surface. The created pairs will be discharged by the small electric field along the magnetic field and this discharge will partially screen the electric field. Because the created pairs lose their perpendicular momentum within very short distance, the Lorentz factor after losing the perpendicular momentum is $\Gamma \sim 1/\sin \theta_0 \sim 10(\sin \theta_a/0.1)^{-1}$. The magnetic pairs will screen the electric field near the inner boundary so that the potential drop between the inner boundary and the point, below which the magnetic pair-creation process is occurred, is reduced to $V \sim 5 \times 10^6$ Volts.

If all field lines in the polar cap region are bending toward the last-open field line, the outgoing magnetic pairs are not expected because the collision angle is always $\alpha < 90^\circ$. In such a case, all pairs created by the magnetic pair-creation process will have an

inward momentum, implying the photon-photon pair-creation process will be only possible mechanism to close the outer gap.

3. Outer gap closed by magnetic pair-creation process

Our gap closure process is summarized as follows;

1. the incoming particles emit ~ 100 MeV photons below the null charge surface,
2. the ~ 100 MeV photons emitted toward the stellar surface will produce the pairs via the magnetic pair-creation process ($M_{e^\pm} \sim 10^4 - 10^5$) above the height $h_{\perp,m}$ estimated by equation (6), and
3. if some fraction of the created pairs will be produced with an outgoing momentum due to the geometry of the local magnetic field, then the outgoing pairs close the outer gap in the trans-field direction everywhere in the outer magnetosphere.

We will discuss the applicability of the present model in section 4.2.

Applying equation (6) as the typical thickness of the gap rescaled at the radial distance $r = R_i$ with the dipole field geometry, we define the fractional gap thickness on the stellar surface as

$$f_m \equiv \frac{h_{\perp,m}(R_s)}{r_p} \sim 0.25K(\chi, B_m, s)P_{-1}^{1/2}, \quad (7)$$

with

$$K = \chi_{-1}^2 B_{m,12}^{-2} s^7 \left(\frac{R_s}{R_i} \right)^{3/2}, \quad (8)$$

Applying the fractional gap thickness to the acceleration and curvature emission process beyond the null charge surface, we discuss the expected properties of the γ -ray

radiation from the outer gap closed by the magnetic pair-creation process. The typical magnitude of the electric field in the gap beyond the null charge surface is given by

$$E_{\parallel}(K, B_d, P) \sim \frac{f_m^2 V_a}{R_{lc}} \sim 8.3 \times 10^4 K^2 B_{d,12} P_{-1}^{-2} \text{ Volt/cm.} \quad (9)$$

which can accelerate the electrons and positrons up to

$$\gamma(K, B_d) \sim \left(\frac{3s^2}{2e} E_{\parallel} \right)^{1/4} \sim 2.1 \times 10^7 K^{1/2} B_{d,12}^{1/4}, \quad (10)$$

where we used $s = R_{lc}$ in the outer magnetosphere. We find that the maximum Lorentz factor does not depend on the rotational period. The typical energy of the curvature radiation by the accelerated particles in the outer magnetosphere is

$$E_c(K, B_d, P) = \frac{3}{4\pi} \frac{hc\gamma^3}{s} \sim 0.55 K^{3/2} B_{d,12}^{3/4} P_{-1}^{-1} \text{ GeV.} \quad (11)$$

Because the efficiency of the emission is significantly reduced above the energy E_c , we expect that the γ -ray spectrum has the cut-off energy of E_c .

The total current flowing in the gap is order of $I_{gap} \sim f_m I_{GJ}$, where $I_{GJ} = \pi B_d R_s / P R_{lc}$ is the Goldreich-Julain current. Using the total potential drop in the gap of $V_{gap} \sim f_m^2 V_a$, we can estimate the γ -ray luminosity as

$$L_{\gamma}(K, B_d, P) \sim I_{gap} V_{gap} \sim 2 \times 10^{33} K^3 B_{d,12}^2 P_{-1}^{-5/2} \text{ erg/s.} \quad (12)$$

4. Application and discussion

4.1. Comparison with *Fermi* observations

The present model predicts the cut-off energy and the luminosity of the γ -ray emissions are related with the stellar magnetic field and the rotation period as $E_c \propto B_d^{3/4} P^{-1}$ of equation (11) and $L_{\gamma} \propto B_d^2 P^{-5/2}$ of equation (12), respectively. We plots the our predictions

with the observations on the cut-off energy in Figure 3 and on the luminosity in Figure 4. In the figures, the circle and triangle symbols represent the radio-selected and γ -ray selected γ -ray pulsars, and the squares are the millisecond pulsars. We can see that the slope of the model prediction is consistent with the observations for both canonical pulsars and millisecond pulsars.

In the present outer gap model, the properties of the γ -ray emissions depend on the local parameters $K(\chi, B_m, s) = \chi_{-1}^2 B_{m,12}^{-2} s_7 (R_s/R_i)^{3/2}$, which is determined by the local magnetic structure. In fact, we adopted $K = 2$ for the canonical γ -ray pulsars and $K = 15$ for the millisecond pulsars in Figures 3 and 4. The strength of the multiple field at a distance δR from the stellar surface may be expressed as $B_m \sim B_s [(\delta r + \delta R)/\delta r]^{-(m+1)}$, where B_s is the strength of the multiple field at the stellar surface and $\delta r \sim 1 - 3 \times 10^5$ cm is the thickness of the crust, the index m is the multiplicity. If we consider the localized dipole field ($m = 2$), $B_m \sim B_s [(\delta r + \delta R)/\delta r]^{-3}$, with $B_s \sim 10^{13}$ Gauss, this localized dipole field becomes same order of magnitude with the global dipole field at about one stellar radius from the stellar surface, because $B_m(r - R_s = R_s) \sim B_s (\delta r/R_s)^3 \sim 10^{-2} B_s$ with $\delta r \sim 2 - 3 \times 10^5$ cm and because the global dipole field becomes $B_d/2^3$ at $r - R_s = R_s$. If the radial distance below which the magnetic pair-creation process takes place is $R_i = 2R_s$, the strength of the magnetic field at R_i is $B_m \sim 10^{11}$ Gauss and the curvature radius of the multiple field will be $s \sim 10^6$ cm. This implies the local parameter of $K = 2^{-3/2} \chi_{-1}^2 B_{m,12}^{-2} s_7 \sim 3.5$, which explains $K \sim 2$ in Figures 3 and 4. For the millisecond pulsars, it is expected that the magnetic pair-creation of the photons with the energy $E_{min} \sim 100$ MeV is possible only at very close to the stellar surface ($r \sim R_s$), because the field strength is about three or four order of magnitude smaller than that of the canonical pulsars. If we adopt $B_s \sim 3 \times 10^{10}$ Gauss as the strength of the multiple field on the stellar surface and $s \sim 10^5$ cm as the curvature radius of the multiple field, we obtain $K \sim 10$.

As Figures 3 and 4 show, the present model predicts that the local parameter $K(\chi, B_m, s)$ discriminates the canonical and the millisecond pulsars as the different populations on the plots of the cut-off energy E_c versus $B_d^{3/4}P^{-1}$ and of the luminosity L_γ versus $B_d^2P^{-5/2}$. From equations (11) and (12), on the other hand, one can see that L_γ/E_c^2 does not include the local factor $K(\chi, B_m, s)$. More strictly speaking, the quantities L_γ/E_c^2 carries away the dependency on the gap thickness f , which depends on the local parameters K , because $L_\gamma \propto f^3 L_{sd}$ and $E_c \propto f^{3/2} V_a^{3/4} s^{-1/4}$. We then obtain the relation that

$$\frac{L_\gamma}{E_c^2} \sim 6.6 \times 10^{34} B_{d,12}^{1/2} P_{-1}^{-1} \text{ erg/s GeV}^2. \quad (13)$$

Figure 5 compares the model prediction and the observations for each pulsar. Figure 5 shows that both canonical pulsars and millisecond pulsars are consistent with the line of $L_\gamma/E_c^2 \propto B_{d,12}^{1/2} P_{-1}^{-1}$. This predicts that although there is a gap between the two populations, where no γ -ray pulsars are plotted in Figure 5, in fact two populations will be continuously connected. It is expected that more γ -ray pulsars having smaller $B_{d,12}^{1/2} P_{-1}^{-1}$ than the present canonical γ -ray pulsars will be discovered by *Fermi* γ -ray telescope. Those pulsars will be expected to distribute around solid line in Figure 5, and two populations, i.e. the canonical and millisecond pulsars, will be continuously connected in the plot.

Recasting the cut-off energy E_c given by equation (11) and the γ -ray luminosity L_γ given by equation (12) as a function of the spin down age $\tau = P/2\dot{P}$, we obtain

$$E_c \sim 7K^{3/2} B_{d,12}^{-1/4} \tau_3^{-1/2} \text{ GeV} \quad (14)$$

and

$$L_\gamma \sim 10^{36} K^3 B_{d,12}^{-1/2} \tau_3^{-5/4} \text{ erg/s}, \quad (15)$$

respectively, where τ_3 is the spin down age in units of 1 kyrs and $L_{sd,34}$ is the spin down power in units of 10^{34} erg/s. Figures 6 and 7 plot the cut-off energy and the γ -ray luminosity as a function of the spin down age, respectively. The lines in Figure 6 and Figure 7 are

results for $K = 2$ and the typical magnetic field of $\langle B_{d,12} \rangle = 3$ for the canonical pulsars (solid lines), and for $K = 15$ and $\langle B_{d,12} \rangle = 3 \times 10^{-4}$ for the millisecond pulsars (dashed lines). We can see that the model predictions are consistent with the observations for both populations. The present model predicts that the two populations will be separated in the plots of the emission properties (E_c, L_γ) as a function of the spin down age.

If we recast the cut-off energy E_c given by equation (11) and the γ -ray luminosity L_γ given by equation (12) as a function of the spin down power $L_{sd} = (2\pi)^4 B_d^2 R_s^6 / 6c^3 P^4$, we obtain

$$E_c \sim 0.31 K^{3/2} B_{d,12}^{1/4} L_{sd,34}^{1/4} \text{ GeV} \quad (16)$$

and

$$L_\gamma \sim 5 \times 10^{32} K^3 B_{d,12}^{3/4} L_{sd,34}^{5/8}, \text{ erg/s} \quad (17)$$

respectively. One can see that the proportionality coefficients $K^{3/2} B_{d,12}^{1/4}$ in equation (16) and $K^3 B_{d,12}^{3/4}$ in equation (17) have less dependency on the pulsar populations. For example, if we apply $K = 2$ and the typical field $\langle B_{d,12} \rangle = 3$ for the canonical pulsars and $K = 15$ and $\langle B_{d,12} \rangle = 3 \times 10^{-4}$ for the millisecond pulsars, we obtain $\langle K^{3/2} B_{d,12}^{1/4} \rangle \sim 3.7$ for the canonical pulsars and ~ 7.6 for the millisecond pulsars, and $\langle K^3 B_{d,12}^{3/4} \rangle \sim 18$ for the canonical pulsars and ~ 7.7 for the millisecond pulsars. We find that the proportionality coefficients between the two populations are different only about factor of two, implying it is difficult to discriminate between the two populations in the plot of the cut-off energy (or γ -ray luminosity) versus the spin down power. Figure 8 and 9 plot the cut-off energy and the γ -ray luminosity as a function of the spin down power, respectively. The solid lines are model predictions with $\langle K^{3/2} B_{d,12}^{1/4} \rangle \sim 5$ in Figure 8 and $\langle K^3 B_{d,12}^{3/4} \rangle \sim 13$ in Figure 9. Figures 8 and 9 show the predicted relations that $E_c \propto L_{sd}^{1/4}$ and $L_\gamma \propto L_{sd}^{5/8}$ are consistent with the observations for both canonical pulsars and millisecond pulsars.

4.2. Applicability to pulsars

In this section, we describe applicability of our model to the pulsars. The present gap closure model invokes the condition that the thickness $h_{\perp,m}$, above which the magnetic pair-creation becomes to be important, is less than the thickness, at which the gap is closed by the photon-photon pair-creation process. To discuss the applicability to the pulsars, for example, one may compare the present model with a self-consistent model investigated by Zhang & Cheng (1997), who discussed the gap thickness closed by the photon-photon pair-creation process. They estimate the fractional gap thickness, which is defined by the ratio between the typical gap thickness at $r = R_{lc}/2$ and the light radius, as $f_p \equiv h_{\perp}(R_{lc}/2)/R_{lc} \sim 5.5P^{26/21}B_{d,12}^{-4/7}$. We recast our fractional gap thickness defined in equation (7) into one in the sense of the definition by Zhang & Chang (1997). Because the trans-field thickness of the magnetic flux tube is approximately proportional to $h_{\perp} \propto r^{3/2}$, the fractional gap thickness is described by $f_{m,1} \equiv h_{\perp,m}(R_{lc}/2)/R_{lc} \sim 2^{-3/2}f_m$, where f_m is defined by equation (7).

We compare the predicted thicknesses of f_p and $f_{m,1}$ for 36 canonical γ -ray pulsars in Table 1 and for 8 millisecond γ -ray pulsars in Table 2. We find that the pulsars with a larger spin down luminosity, such like PSR J0534+2200 (the Crab pulsar), has $f_p \ll f_{m,1}$. As Table 1 and Table 2 show, on the other hand, the mature pulsars, such like PSR J0633+1746 (the Geminga pulsar), and the millisecond pulsars, who show a smaller spin down power, indicate $f_p \gg f_{m,1}$.

The present gap closure process with the magnetic pair-creation process will be applicable for the pulsars whose have $f_{m,1} \lesssim f_p$, that is, the predicted gap thickness $f_{m,1}$ is comparable with or slightly less than f_p of the photon-photon pair-creation process. The condition that $f_p \ll f_{m,1}$ implies that the efficient photon-photon pair-creation will definitely close the gap before the gap reaches the thickness $f_{m,1}$. For the case $f_p \gg f_{m,1}$,

on the other hand, the outer gap must be thicker than f_m , but the gap may be closed by magnetic pair-creation process with the thickness at which the photon-photon pair-creation is initiated in the gap. Equating the fractional gap thickness f_p and $f_{m,1}$, it may be suggested that the switching of the gap closure mechanism takes place at

$$L_{sd} \sim 2.5 \times 10^{36} (K/2)^{-168/31} B_{d,12}^{-34/31} \text{ erg/s}, \quad (18)$$

indicating the photon-photon pair-creation closes the gap for the pulsars with $L_{sd} \gtrsim 10^{36}$ erg/s, while the magnetic pair-creation may close the gap for $L_{sd} \lesssim 10^{36}$ erg/s.

4.3. Validity of assumption

In the present model, we assume that the energy loss due to the curvature radiation below the null charge surface is not compensated by the acceleration of the electric field in the gap. For simplicity, we assume that the electric field decreases quadratically along the field lines below the null charge surface toward the inner boundary;

$$E_{||}(r < R_n) = \frac{(r/R_{in})^2 - 1}{(R_n/R_{in})^2 - 1} E_{||,0}, \quad (19)$$

where R_{in} and R_n are the radial distance to the inner boundary and the null charge point, respectively, and $E_{||,0}$ is the electric field at the null charge point, which is characterized by equation (9). If the inner boundary is located ~ 1 stellar radius from the stellar surface, the acceleration field is reduced to $E_{||}(r \sim R_{in}) \sim (R_{in}/R_n)^2 E_{||,0} \sim 10^{-2} E_{||,0}$ near the inner boundary. Applying the typical electric field described by equation (9) at the null charge point, a particle gains energy by the electric field with a rate of

$$eE_{||}(r \sim R_{in})c \sim 40K^2 B_{d,12} P_{-1}^{-2} \text{ erg/s}. \quad (20)$$

On the other hand, the particles having the Lorentz factor expressed by equation (2) lose their energy via the curvature radiation with a rate of

$$P_c = \frac{2}{3} \gamma^4 \frac{e^2 c}{s^2} \sim 5 \times 10^3 s_7^{-2/3} \text{ erg/s}, \quad (21)$$

indicating the energy loss by the curvature radiation dominates the energy gain by the acceleration of the electric field. In fact, (1) the electrodynamic model expects the electric field will decrease more rapidly below the null charge surface than the quadratic expression (Hirotani 2006a) or (2) the inner boundary will be located far from the stellar surface for the small current case. Therefore we can safely assume that the energy loss due to the curvature radiation below the null charge surface is not compensated by the acceleration of the electric field.

4.4. Comparison with the previous works

We briefly summarize the difference in the predicted γ -ray luminosity between the present model and the model investigated by Zhang & Cheng (1997). Zhang & Cheng (1997) predicted the fractional gap thickness $f_p \sim 5.6P^{26/21}B_{d,12}^{-4/7}$ of the outer gap closed by the photon-photon pair-creation process in the outer magnetosphere. With this model, the γ -ray luminosity depends on the spin down power as $L_\gamma \propto B_d^{1/7}L_{sd}^{1/14}$. Therefore, the γ -ray luminosity is less dependent on the spin down power. Later, they developed their gap model by taking into account the effects of the inclination angle between the rotation axis and the magnetic axis (Zhang et al. 2004). They argued that the fractional gap thickness and the resultant γ -ray luminosity depend on the inclination angle. They assumed that when the fractional gap thickness goes to unity, then the γ -ray luminosity approaches to the spin down power. Therefore, the γ -ray luminosity is bounded between $L_{sd}^{1/14}$ and L_{sd} depending on the inclination angle. They carried out a Monte Carlo simulation to calculate the γ -ray luminosity by assuming that the inclination angle is randomly distributed. As a result, they obtained the relation that $L_\gamma \propto L_{sd}^\beta$ with an index of $\beta = 0.38 \sim 0.46$. In the present model, on the other hand, the fractional gap thickness $f_m \propto P^{1/2}$ has a less dependency on the rotational period compared with the model of Zhang & Cheng (1997), in which

$f_p \propto P^{26/21}$. As a result, without introducing the effects of the inclination angle, the present model predicts the relation of $L_\gamma \propto L_{sd}^\beta$ with more steep index of $\beta = 5/8$.

5. Conclusion

In this paper, we have studied the outer gap accelerator model closed by magnetic pair-creation process. We argued that below null charge surface, the curvature loss is not compensated by the acceleration due to the electric field in the gap. In such a case, the incoming particles, which were produced in the outer magnetosphere, will emit curvature photons with about $E_{min} \sim m_e c^2 / \alpha_f \sim 100$ MeV. The 100 MeV curvature photons propagating toward the stellar surface will be converted into pairs by the pair-creation process with the strong local magnetic field near the stellar surface, where the multiple magnetic field affects to the global field lines. For the canonical pulsar, the synchrotron radiation of the created pairs produce ~ 5 MeV photon, which will be furthermore converted into pairs. As a result, multiplicity of an incoming particle could acquire $M_{e^\pm} \sim 10^4 - 10^5$. With the local field lines bending away from the last-open field line (such as illustrated in Figure 2), the created pairs via the magnetic pair-creation process can have the outgoing momentum and migrate into the outer magnetosphere. If ~ 10 pairs out of $M_{e^\pm} \sim 10^4 - 10^5$ migrate outward to the outer magnetosphere, those pairs could close the outer gap accelerator. According to this scenario, the main results of this paper are as follows. The fractional thickness of the outer gap becomes $f_m \sim 0.25 K P_{-1}^{1/2}$, which has a less dependency on the rotational period compared with the outer gap model proposed by Zhang & Cheng (1997). With the present model, the spectral properties of the γ -ray emissions depend on the local parameter $K \sim \chi_{-1}^2 B_{m,12}^{-2} s_7 (R_s/R_i)^{3/2}$, which is determined by the local magnetic structure near the star. We expect that the local parameter K takes a value of $K \sim 2$ for the canonical pulsars and $K \sim 15$ for the millisecond pulsars (Figures 3 and 4). The present

model predicts that the canonical pulsars and the millisecond pulsars are connected in the plots of L_γ/E_c versus $B_s^{1/2}P^{-1/2}$, in which the effect of the fractional gap thickness is carried away (Figure 5). The present model predicts that the cut-off energy (E_c) and the γ -ray luminosity (L_γ) depend on the spin down age or the spin down power as $E_c \propto \tau^{-1/2}$ and $L_\gamma \propto \tau^{-5/4}$ or $E_c \propto L_{sd}^{1/4}$ and $L_\gamma \propto L_{sd}^{5/8}$ (Figures 6-9).

In addition to the cut-off energy and γ -ray luminosity, which have been discussed in this paper, the *Fermi* γ -ray telescope provides the photon index of γ -ray spectrum and the pulse profiles for each pulsar (Abdo et al. 2010). It must be important to discuss the photon index and the pulse profile with the acceleration model, because they will contain information of the electric structure (e.g. the distribution of the electric field) in the acceleration region and the three-dimensional geometry of the emission region (e.g. Romani & Yadigaroglu 1995; Cheng, Ruderman & Zhang 2000; Spitkovsky 2006). However, a more detail model, which has to consider the electrodynamics in the gap and three-dimensional structure, is required to study the shape of the γ -ray spectra and the pulse profiles. Studying the emission properties with the electrodynamics in the present outer gap closure model will be done in the subsequent papers.

We wish to express our thanks to the referee for insightful comments on the manuscript. We thank the useful discussions with H.-K. Chang, K. Hirotani, C.Y. Hui, B. Rudak, M.Ruderman and S.Shibata. We also thank to Theoretical Institute for Advanced Research in Astrophysics (TIARA) operated under Academia Sinica Institute of Astronomy and Astrophysics, Taiwan, which enables author (J.T.) to use PC cluster at TIARA. This work is supported by a GRF grant of Hong Kong SAR Government under HKU700908P.

REFERENCES

- Abdo A.A. et al., 2010, *ApJS*, 187, 460
- Abdo A.A. et al., 2009b, *Sci.*, 325, 848
- Abdo A.A. et al., 2009c, *Sci.*, 325, 840
- Abdo A.A. et al., 2009d, *ApJ*, 696, 1084
- Aliu E. et al., 2008, *Sci*, 322, 1221
- Arons J., 1993, *ApJ*, 408, 160
- Arons J., 1983, *ApJ*, 266, 215
- Blandford R.D., Applegate J.H. & Hernquist, L., 1983, *MNRAS*, 204, 1025
- Cheng K.S., Ruderman M. & Zhang L. 2000, *ApJ*, 537, 964
- Cheng K.S., Ho C. & Ruderman M. 1986a, *ApJ*, 300, 500
- Cheng K.S., Ho C. & Ruderman M. 1986b, *ApJ*, 300, 522
- Goldreich P. & Julian W.H. 1969, *ApJ*, 157, 869
- Daugherty J.K. & Harding, A.K., 1996, *ApJ*, 458, 278
- Daugherty J.K. & Harding, A.K., 1982, *ApJ*, 252, 337
- Dyks J. & Rudak B., 2003, *ApJ*, 598, 1201
- Dyks J., Rudak B. & Harding A.K., 2004, *ApJ*, 607, 939
- Erber T., 1966, *RvMP*, 38, 626
- Harding A.K., Stern J.V., Dyks J. & Frackowiak M., 2008, *ApJ*, 680, 1378

- Harding A.K., Usov V.V., Muslimov A.G., 2005, ApJ, 622, 531
- Hirotsu K., Harding A.K. & Shibata S., 2003, ApJ, 591, 334
- Hirotsu K., 2008, ApJL, 688, 25
- Hirotsu K., 2006a, ApJ, 652, 1475
- Hirotsu K., 2006b, Mod. Phys. Lett. A, 21, 1319
- Hirotsu K. & Shibata S., 2001, ApJ, 558, 216H
- Pellizzoni, A. et al., 2009, ApJ, 695, 115
- Romani R.W. & Yadigaroglu I.-A. 1995, ApJ, 438, 314
- Romani R.W, 1990, Nature, 347, 741
- Ruderman M., 1991, ApJ, 366, 261
- Ruderman M.A. & Sutherland P.G., 1975, ApJ, 196, 51
- Spitkovsky A., 2006, ApJL, 648L, 51
- Tang P.S. Anisia, Takata J., Jia, J.J., Cheng K.S., 2008, ApJ, 676, 562
- Takata J. & Chang H.-K., 2009 MNRAS, 392, 400
- Takata J. & Chang H.-K., 2007 ApJ, 670, 677
- Takata J., Chang H.-K. & Cheng K.S., 2007 ApJ, 656, 1044
- Takata J., Shibata S. & Hirotsu K. 2004, MNRAS, 354, 1120
- Thompson D.J., 2004, in Cheng K.S., Romero G.E., eds, Cosmic Gamma Ray Sources.
Dordrecht, Kluwer, p. 149

Venter C., Harding A.K. & Guillemot L., 2009, ApJ, 707, 800

Zhang L., Cheng K.S., Jiang Z.J. & Leung P., 2004, ApJ, 604, 317

Zhang L. & Cheng K.S., 2003, A& A 398, 639

Zhang L. & Cheng K.S., 1997, ApJ, 487, 370

Name	$P(s)$	$B_d(10^{12} \text{ G})$	$L_{sd}(10^{34} \text{ erg/s})$	f_p	$f_{m,1}; K = 2$
J0534+2200	0.033	3.8	46100	0.038	0.10
J1833–1034	0.062	3.5	3370	0.085	0.14
J0205+6449	0.066	3.6	2700	0.091	0.14
J2229+6114	0.052	2.0	2250	0.093	0.13
J1124–5916	0.135	10.0	1190	0.12	0.21
J1420–6048	0.068	2.4	1000	0.12	0.15
J0835–4510	0.089	3.4	688	0.14	0.17
J1813–1246	0.048	0.9	626	0.13	0.12
J1418–6058	0.11	4.4	495	0.16	0.19
J1952+3252	0.040	0.5	374	0.15	0.11
J1826–1256	0.11	3.7	358	0.17	0.19
J1709–4429	0.102	3.0	341	0.17	0.18
J2021+3651	0.104	3.2	338	0.17	0.18
J1907+06	0.107	3.1	284	0.18	0.18
J1747–2958	0.990	2.5	251	0.19	0.18
J1048–5832	0.124	3.5	201	0.20	0.20
J1718–3825	0.075	1.0	125	0.22	0.15
J1459–60	0.103	1.6	91.9	0.25	0.18
J2238+59	0.163	4.1	90.3	0.26	0.23
J1028–5819	0.091	1.2	83.2	0.25	0.17
J1509–5850	0.089	0.9	51.5	0.29	0.17
J0007+7303	0.316	10.6	45.2	0.34	0.31
J1809–2332	0.147	2.2	43	0.32	0.21
J1958+2846	0.29	8.0	35.8	0.36	0.30

Name	$P(s)$	$B_d(10^{12} \text{ G})$	$L_{sd}(10^{34} \text{ erg/s})$	f_p	$f_{m,1}; K = 2$
J2032+4127	0.143	1.7	26.3	0.37	0.21
J0248+6021	0.217	3.4	21	0.41	0.26
J0631+1036	0.288	5.5	17.3	0.45	0.30
J0742–2822	0.167	1.7	14.3	0.45	0.23
J1732–31	0.197	2.2	13.6	0.46	0.25
J0633+0632	0.297	4.8	11.9	0.50	0.30
J2021+4026	0.265	3.8	11.6	0.50	0.29
J2043+2740	0.096	0.3	5.6	0.55	0.17
J0659+1414	0.385	4.3	3.8	0.73	0.35
J0633+1746	0.237	1.6	3.3	0.71	0.27
J1057–5226	0.197	1.1	3	0.70	0.25
J1836+5925	0.173	0.5	1.2	0.92	0.23
J1741–2054	0.414	2.3	0.9	1.14	0.36
J0357+32	0.444	1.9	0.5	1.40	0.37

Table 1: Pulsar parameters, which were taken from Abdo et al. (2010), and the fractional gap thickness predicted by Zhang & Cheng (1997), f_p , and by the present model, $f_{m,1}$, for 38 canonical γ -ray pulsars. Here, the fractional gap thickness is defined by the ratio between the typical gap thickness at $r = R_{lc}/2$ and the light radius.

Name	$P(ms)$	$B_d(10^8 \text{ G})$	$L_{sd}(10^{34} \text{ erg/s})$	f_p	$f_{m,1}; K = 15$
J0218+4232	2.3	4.1	24	0.26	0.20
J0613–0200	3.1	1.8	1.3	0.60	0.23
J0751+1807	3.5	1.5	0.6	0.76	0.25
J1614–2230	3.2	1.2	0.5	0.78	0.24
J1744–1134	4.1	1.8	0.4	0.84	0.27
J2124–3358	4.9	2.4	0.4	0.89	0.29
J0030+0451	4.9	2.2	0.3	0.92	0.29
J0437–4715	5.8	2.9	0.3	0.98	0.32

Table 2: Pulsar parameters, which were taken from Abdo et al. (2010), and the fractional gap thickness predicted by Zhang & Cheng (1997), f_p , and by the present model, $f_{m,1}$, for 8 millisecond γ -ray pulsars. Here, the fractional gap thickness is defined by the ratio between the typical gap thickness at $r = R_{lc}/2$ and the light radius.

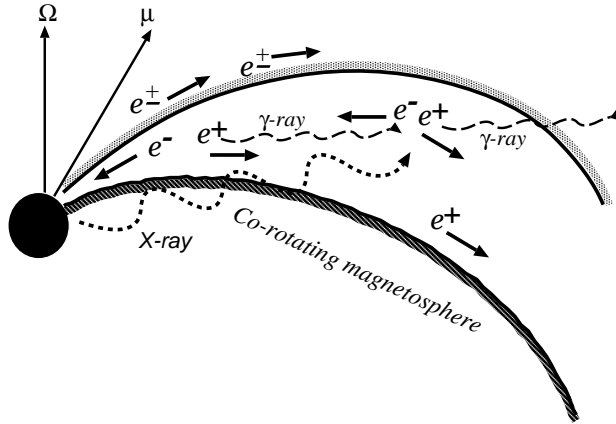


Fig. 1.— Schematic view of the outer gap accelerator. In the outer magnetosphere, the photon-photon pair-creation process produce the pairs in the gap uniformly. The pairs created by the magnetic pair-creation process close the outer gap in the outer magnetosphere. The favorable magnetic structure near the stellar surface is depicted in Figure 2.

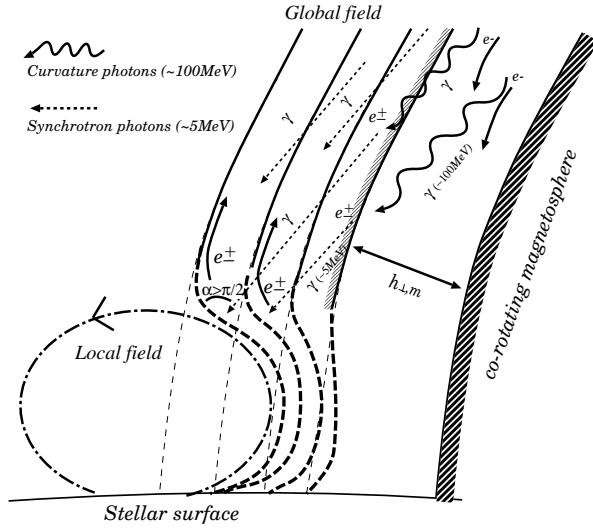


Fig. 2.— Schematic view of the favorable magnetic structure near the stellar surface.

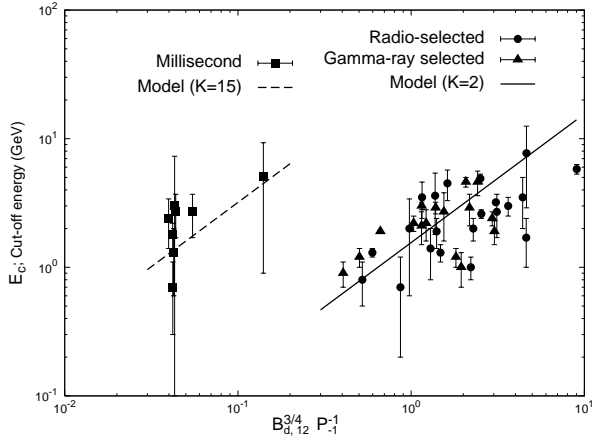


Fig. 3.— Plot of the cut-off energy as a function of $B_{d,12}^{3/4} P_{-1}^{-1}$. The circle and triangle symbols are observations for the radio-selected and the γ -ray selected γ -ray pulsars, respectively. In addition, the square symbols represent the millisecond pulsar. The solid and dashed lines show the prediction of the model, $E_c = 0.55K^{3/2} B_{d,12}^{3/4} P_{-1}^{-1}$ GeV of equation (11). The model results are for $K = 2$ for the canonical pulsar (solid line) and $K = 15$ for the millisecond pulsars (dashed line). The observations are taken from Abdo et al. (2010).

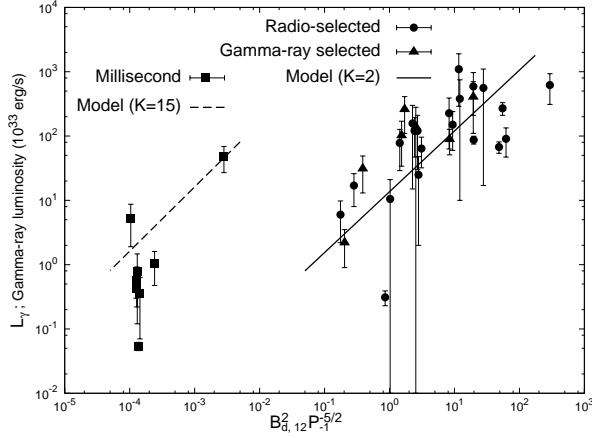


Fig. 4.— Plot of the γ -ray luminosity as a function of $B_{d,12}^2 P_{-1}^{-5/2}$. The symbols correspond to same case as Figure 3. The lines represent the model prediction, $L_\gamma \sim 2 \times 10^{33} K^3 B_{d,12}^2 P_{-1}^{-5/2}$ erg/s of equation (12), with $K = 2$ for the canonical pulsar (solid line) and $K = 15$ for the millisecond pulsars (dashed line).

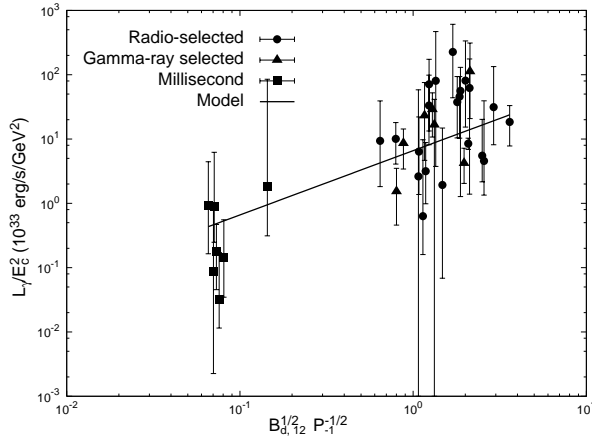


Fig. 5.— Plot of L_γ/E_c^2 as a function of $B_{d,12}^{1/2} P_{-1}^{-1/2}$. The symbols correspond to same case as Figure 3. The line corresponds to the model prediction, $L_\gamma/E_c^2 \sim 6.6 \times 10^{34} B_{d,12}^{1/2} P_{-1}^{-1}$ erg/s GeV^2 of equation (13).

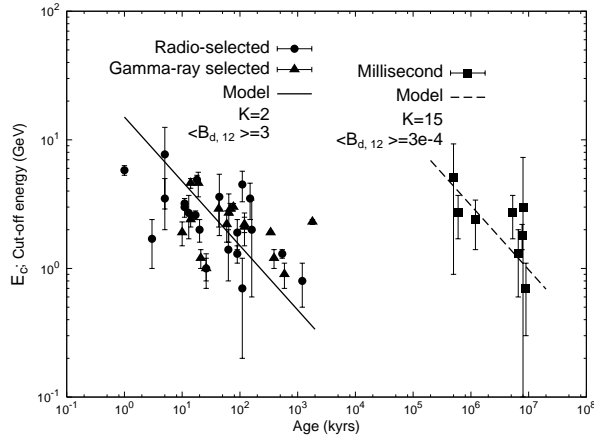


Fig. 6.— Plot of the cut-off energy as a function of the spin down age. The symbols correspond to same case as Figure 3. The lines correspond to the model prediction, $E_c \sim 7K^{3/2}B_{d,12}^{-1/4}\tau_3^{-1/2}$ GeV of equation (14), with $K = 2$ and the typical magnetic field $\langle B_{d,12} \rangle = 3$ for the canonical pulsars (solid line), and $K = 15$ and $\langle B_{d,12} \rangle = 3 \times 10^{-4}$ for the millisecond pulsars (dashed line).

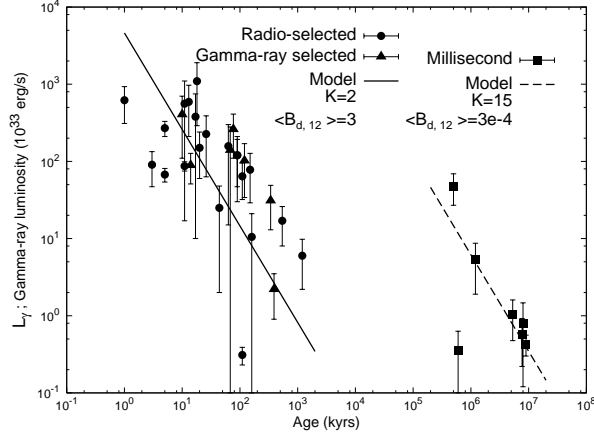


Fig. 7.— Plot of the γ -ray luminosity as a function of the spin down age. The symbols correspond to same case as Figure 3. The lines correspond to the model prediction, $L_\gamma \sim 10^{36} K^3 B_{d,12}^{-1/2} \tau_3^{-5/4}$ erg/s of equation (15), with $K = 2$ and $\langle B_{d,12} \rangle = 3$ for the canonical pulsars (solid line), and $K = 15$ and $\langle B_{d,12} \rangle = 3 \times 10^{-4}$ for the millisecond pulsars (dashed line).

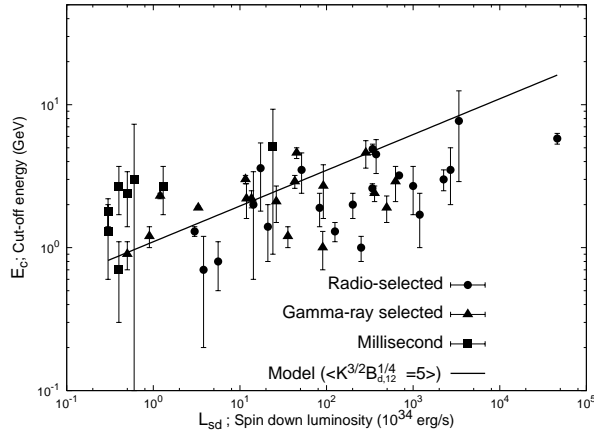


Fig. 8.— Plot of the cut-off energy as a function of the spin down power. The symbols correspond to same case as Figure 3. The line is the model prediction, $E_c \sim 0.22 K^{3/2} B_{d,12}^{1/4} L_{sd,34}^{1/4}$ GeV of equation (16), with $\langle K^{3/2} B_{d,12}^{1/4} \rangle = 5$.

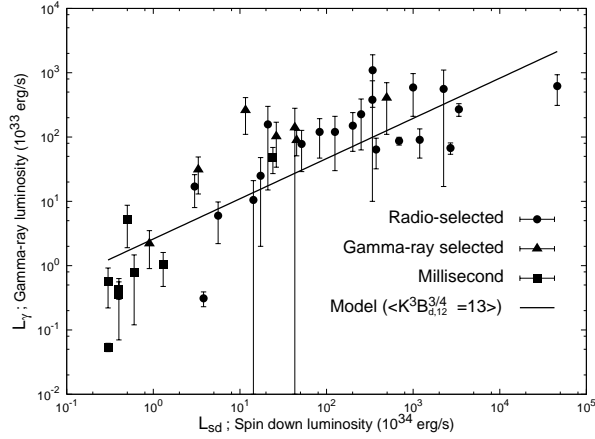


Fig. 9.— Plot of the γ -ray luminosity as a function of the spin down power. The symbols correspond to same case as Figure 3. The line is the model prediction, $L_\gamma \sim 2 \times 10^{32} K^3 B_{d,12}^{3/4} L_{sd,34}^{5/8}$ erg/s of equation (17), with $\langle K^3 B_{d,12}^{3/4} \rangle = 13$.